An active thermographic technique for highly resolved heat transport measurements in paper drying

D. BANERJEE[1], C. S. GARBE[2], U. SCHIMPF[3], B. JÄHNE[2], S. SCHABEL[1]

1 Chair for Paper Technology and Mechanical Process Engineering, Darmstadt University of Technology, Alexanderstrasse 8, D-64283, Darmstadt, Germany.
2 Interdisciplinary Centre for Scientific Computing, University of Heidelberg, Im Neuenheimer Feld 368, Heidelberg D-69120, Germany.
3 Institute of Environmental Physics, University of Heidelberg, Im Neuenheimer Feld 229, Heidelberg D-69120, Germany.

Keywords: Thermography, paper drying, spatial resolution, heat capacity, amplitude damping, phase shifts, Lock-in thermography, heat transfer velocity.

ABSTRACT
A novel measurement technique, based on infrared thermography, has been applied for characterizing the thermal properties of paper with high spatial resolution. The technique is termed as 'active thermography' since the temperature response of a paper sheet is observed and analyzed with respect to an external periodic heating. Through the analysis of the temperature response of the paper surface in the Fourier domain for different modulation frequencies of incident heat flux, heat transfer velocities across the solid-gas interface can be estimated. This in turn results in estimation of the heat capacity of paper by solving the heat balance equations of the system. The thermal heating is applied spatially homogeneously. Therefore all these calculations are performed for all pixels in the image sequence. A spatial distribution and temporal development of all these parameters were visualized. Also the technique shows high potential to the non-invasive dynamic measurements in paper drying.

1 INTRODUCTION

Paper drying is the most energy intensive process of paper production. With the increasing demand of uniformity and the introduction of new process steps in high-speed production of paper, a more detailed inspection of paper properties is desirable which could provide local properties of paper within a small area. This uniformity can be in terms of optical, chemical or thermal properties which in turn will affect the process performance and end use. The existing monitoring techniques of these parameters give either integrated or point measurement with no resolution in space. Point measurements can give higher resolution in time. However they do not give spatial resolution. Hence a more detailed inspection of paper properties is desirable. For instance in printing, the interaction of ink droplets with paper is in micrometer (or even smaller) scale and is governed by local paper properties. Therefore, much higher resolution will be necessary for the next generation monitoring systems [1]. This is also necessary for the development of much more accurate theoretical models for the processes involved.

With the advancement and availability of modern low noise infrared cameras, the wide spread application of thermographic measurements to a vast field of science has become feasible. This makes non-invasive measurement of physical parameters possible at high spatial and temporal resolution. These aspects have become highly relevant with the increasing awareness of the importance of dynamic processes and their distribution in many fields of science. The application of infrared techniques in the field of paper engineering has gained substantial attention both in production as well as scientific research [2-5]. Infrared imaging has been applied extensively in trouble shooting, diagnostics and condition monitoring [6-9]. Charles [10] has applied a high speed line scanned infrared imaging to perform diagnostics on a Yankee dryer and on a size press in newsprint machine. He also reported the use of an infrared camera for cockle detection. In a study by Yamauchi and Murakami [11], the fracture patterns and crack propagation in notched hand sheets were studied by infrared thermography. Forester et al. [12] reported on an application of infrared thermography for the identification of substances suitable for the detection of stickies. Hojjatie et al. [13] investigated the in-plane distribution of moisture in paper by infrared thermography. Industrial applications of infrared imaging involved estimation of temperature and moisture distribution of paper and condition monitoring of machines.

In this paper, the implementation of a novel measurement technique based on lock-in thermography will be discussed. This approach is inspired by Jähne et al. [14] who developed a similar technique for estimating transfer velocities at the ocean surface and by Garbe et al. [15] who employed thermography for measuring water relations in plant leaves. Initially the underlying equations are presented followed by measurement technique and obtained results.

2 HEAT FLUX EQUATIONS

The temperature of the paper sheet is the net result of several energy fluxes into and out of the system. The magnitude of these fluxes is determined by a set of external and internal parameters. In the following section, the energy balance equation will be deduced to determine heat capacity from infrared image sequences [15].

2.1 Paper sheet energy balance equations:

According to first law of thermodynamics, the total energy in a closed system must be conserved. It may only change in

forms. Therefore, the simple formulation of the energy balance of paper is given by

Energy stored = energy influx + energy efflux. (1)

Influx of energy results from absorbed radiation from the entire spectrum. Heat conduction or convection can either be influx or efflux, depending on the temperature. Additionally paper itself will radiate according to the Stefan-Boltzmann law. Taking all these fluxes into consideration, the above equation can be rewritten as

$$j_{net} = j_{ir} + j_{sen} + j_{lat}, \quad (2)$$

where all the energy fluxes are expressed as flux densities (Wm^{-2}). The component fluxes in the above equation can be derived as follows:

Net energy flux:
The net energy flux j_{net} which causes the temperature change of the object is given by

$$j_{net} = \frac{\Phi}{A} = \frac{1}{A}\frac{dQ}{dt} = \frac{C}{A}\frac{dT}{dt}, \quad (3)$$

which directly relates the temporal temperature change to the net heat flux.

Infrared radiation:
Every object emits thermal radiation. According to the Stefan-Boltzmann law, the flux due to infrared absorption and radiation is given by

$$j_{ir} = 2\alpha_{ir}\sigma(T_{surr}^4 - T_{paper}^4), \quad (4)$$

considering the surrounding to be an object of estimated temperature T_{sur}.

Conduction and Convection:
At the interface between solid-gas, a boundary layer exists, over which the heat is transferred by conduction. Beyond the boundary layer, the heat is transported away from the paper by turbulent convection. This is generally a very fast process, which makes the conductive part the main resistance for sensible heat transport.

Considering heat transport to the paper surface, this sensible heat flux is given by Fourier heat transfer law

$$j_{diff}^{heat} = -D\rho c_p \frac{dT}{dx}. \quad (5)$$

The transfer velocity k_{heat} can be defined as the ratio of the diffusion coefficient D to the diffusion length Δx by

$$k_{heat} = -\frac{D}{\Delta x}. \quad (6)$$

The heat flux over the paper-air boundary layer can then be expressed as follows, with the factor of two for both surfaces

$$j_{sen} = -2k_{heat}\rho c_p (T_{paper} - T_{air}). \quad (7)$$

The direction of this heat flow of course depends on the temperature difference between air and paper.

Evaporation cooling:
The moisture present in the paper sheet will evaporate and thus consume considerable amount of latent heat. Using Fick's law, the mass flux can be calculated as

$$j_{wv} = -D_{wv}\frac{\Delta c_{wv}}{\Delta x} = k_{wv}\Delta c_{wv}. \quad (8)$$

The heat loss is calculated as the product of flux and heat of evaporation of water by

$$j_{lat} = -\lambda j_{wv}. \quad (9)$$

Substituting all these equations in Equation (2) results in

$$\left(\frac{C}{A}\right)_{paper}\frac{dT_{paper}}{dt} = 2\alpha_{ir}^{paper}\sigma(T_{surr}^4 - T_{paper}^4) + 2k_{heat}^{paper}\rho c_p (T_{air} - T_{paper}) + k_{wv}\lambda c_{wv}(h_{paper} - h_{air}) \quad (10)$$

3 EXPERIMENTAL TECHNIQUE

3.1 Theory of Controlled Flux Technique

In the controlled flux technique, a known heat flux is applied to a probe and the transfer velocity is determined either by measuring the concentration difference across the mass boundary layer or from the time constant of transfer across it. In this technique, heat is used as tracer and infrared imaging for visualization and quantitative measurements. Acquired images produce measurements with high spatial and temporal resolution. With thermographic techniques, there are two ways of determining the transfer velocity. In one case, a constant flux is applied and the temperature response is observed. The second way is to measure the temporal response of the mass boundary layer by periodically changing the heat flux. This could either be a short pulse or a periodic variation.

Essentially, this technique applies methods of linear system theory to investigate the transfer process through the boundary layers. The amplitude attenuation and phase shift of the periodic temperature variation at the surface (the output of the 'black box') is measured as a function of the frequency of the periodically varying heat flux (the input).

The heat capacity of paper can be measured spatially resolved by active thermography. The energy balance equation of the paper is given by Equation (10).

Assuming $T_{surr} = T_{air}$ and by substituting $T(t) = T_{air} - T_{paper}(t)$, this equation can be simplified to

$$-\frac{d}{dt}T(t) \approx \left(\frac{A}{C}\right)_{paper}\begin{bmatrix} j_{lat} + j_{act}(t) \\ +(8\alpha_{ir}^{paper}\sigma T_{air}^3 \\ +2\rho c_p k_{heat}^{paper})T(t) \end{bmatrix}. \quad (11)$$

Here we assumed that $T_{air}^4 - T_{paper}^4(t) \approx 4T_{air}^3 T(t)$, which is valid for small T(t). In the above equation an additional flux $j_{act}(t)$ is introduced, accommodating the actively controllable heat source.

Equation (11) can be rewritten as

$$\frac{d}{dt}T(t) = -\frac{1}{\tau}T(t) - b - z(t), \quad (12)$$

where the following substitutions are made in Equation (11)

$$\tau^{-1} \equiv \left(\frac{A}{C}\right)_{paper}(8\alpha_{ir}^{paper}\sigma T_{air}^3 + 2\rho c_p k_{heat}^{paper}), \quad (13)$$

$$b \equiv \left(\frac{A}{C}\right)_{paper}(j_{lat}), \quad (14)$$

$$z(t) \equiv \left(\frac{A}{C}\right)_{paper} j_{act}(t). \quad (15)$$

When *z(t)* is chosen appropriately, Equation (12) can be solved easily. Two choices of z(t) are discussed here, a step change in $j_{act}(t)$ and a periodic variation.

Constant flux method:
In this method, the laser is switched on at t = 0. This results in a constant additional flux j_{act} for t > 0. The paper temperature reaches a new equilibrium with time. The solution for Equation (12) in this case is

$$T(t) = T^{\infty} + \Delta T e^{-t/\tau}, \quad (16)$$

where T^{∞} is the temperature difference between air and paper in the new steady state and ΔT is the temperature increase of the paper due to the additional flux. For actually measuring the temperature response of a paper sheet with respect to the incident heat flux j_{act}, Equation (16) can be expressed in absolute temperatures. Substituting $T = T_{air} - T_{paper}(t)$ leads to

$$T_{paper}(t) = T_{paper}^{\infty} - \Delta T e^{-t/\tau}. \quad (17)$$

The purpose of this method is to attain spatially highly resolved measures of the parameters $T_{paper}^{\infty}, \Delta T$ and τ, which can be achieved with the help of a single infrared camera. Image sequences are acquired synchronized with switching on the heat flux j_{act} at the time t = 0. The temperature change of the paper sheet is recorded with a spatial and temporal resolution of the infrared camera. The exponential function of Equation (17) can then be fitted to the temporal change of temperature of each individual pixel using *Levenberg-Marquardt* nonlinear least squares fit. In this way, spatially highly resolved estimates of the three parameters of the Equation (17) are obtained.

Solving Equation (13) results in an estimation for the heat capacity per unit area of paper under observation by

$$\left(\frac{C}{A}\right)_{paper} = \tau\left(8\alpha_{ir}^{paper}\sigma T_{air}^3 + 2\rho c_p k_{heat}^{paper}\right). \quad (18)$$

The heat capacity can be obtained from the knowledge of the transfer velocity. All the other parameters are either standard material properties or already measured. The transfer velocities can be obtained from using the periodic flux method which is described below.

Periodic Flux Method:
A varying heat flux is $j_{act}(t)$ is applied by switching the laser periodically on and off. The image sequences were obtained for different frequencies. The data obtained in this way was then processed in the frequency domain. The Fourier transform theory states

$$\frac{\partial f(t)}{\partial t} \leftrightarrow i\omega\hat{f}(k), \quad (19)$$

that is, a time derivative of a function in the time domain becomes a multiplication of the Fourier transform of this function with $i\omega$ in the frequency domain. Applying this to Equation (12) yields

$$i\omega\delta\hat{T}(\omega) = -\frac{1}{\tau}\delta\hat{T}(\omega) - \hat{b} - \hat{z}(\omega)\,. \qquad (20)$$

Assuming constant energy flux j_{in} and j_{lat} and constant air temperature T_{air}, this can be rewritten for $\hat{T}_{paper}$ as follows

$$\hat{T}_{paper}(\omega) = \frac{\hat{z}(\omega)}{\frac{1}{\tau} + i\omega}\,. \qquad (21)$$

The phase and amplitude of this complex quantity are

$$\varphi(\omega) = -\arctan(\omega\tau) \text{ and}$$
$$\left|\hat{T}_{paper}(\omega)\right| = \sqrt{\frac{\left|\hat{z}(\omega)\right|^2}{\frac{1}{\tau^2} + \omega^2}}\,. \qquad (22)$$

For $\omega << 1/\tau$ when the period of the input laser signal is much longer than the time constant of the paper system, the phase becomes

$$\varphi(\omega) \approx -\omega\tau\,. \qquad (23)$$

In principle, a measurement of phase yields a value for τ and therefore the heat capacity can be calculated from Equation (18).

The variation of the heat flux with a laser resulted in a periodic rectangular function. As the Fourier spectrum of the rectangular function consists of all odd harmonics, this can be considered as an application of several frequencies (of decreasing amplitude) at once. Experiments were carried out for different laser frequencies from 0.0025 Hz to 1Hz, which corresponds to period lengths of 400s to 1s. For the base frequencies and two of its overtones, the Fourier transform was performed in the time direction. This resulted in parameter images containing the amplitude and the phase shift of the temperature signal of the paper sheet.

Another approach to the determination of transfer velocity was to look at the spectral amplitude attenuation or phase shifts to the different incident laser frequencies. At lower frequency at equilibrium the amplitude damping between the input and the output signal was almost constant whereas at higher frequencies the damping increases. The cutoff frequency between these two parts of the curve will give the corresponding time constant of the system.

3.2 Setup

For the active thermographic technique an additional energy flux $j_{act}(t)$ has to be applied on the paper surface. For this purpose a CO_2 laser of 10.6 µm wavelength was used. To avoid reflections in the thermal images the sensitivity of the camera was chosen to be far beyond the wavelength of the laser. The infrared camera used for the measurements described in this paper is a Raytheon Amber Radiance I MWIR camera. The InSb detector is sensitive in the wavelength range of 3-5 µm. The noise level of the camera is characterised by a Noise Equivalent Temperature Difference (NETD) of 25 mK. The detector is a square Focal Plane Array (FPA) with a resolution of 256 X 256 pixels. The camera is capable of a frame rate of 60 Hz.

In order to achieve a uniformly heated area of paper, the laser beam was expanded with a cylindrical lens and a scanning mirror was used in the optical path as shown in **Figure 1**.

With the help of a multifunction I/O card, the camera and laser were synchronized through the frame grabber card. The synchronisation is important for an accurate estimation of phase shifts in between heating source and paper response.

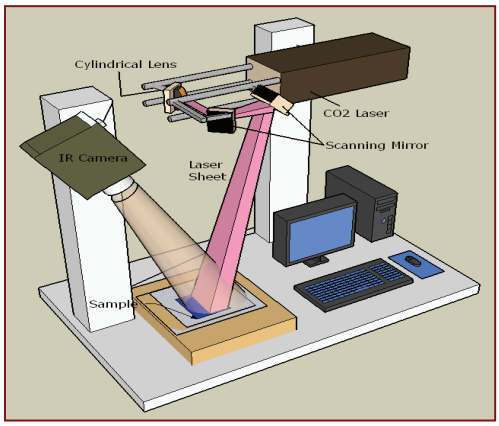

Figure1: *Experimental setup for thermographic measurements*

Laboratory hand sheets were prepared from spruce sulphite pulp. A grammage of 80 gram per square meter and an average thickness of 100 µm have been used for the measurements presented here. The pulp was beaten to different consistency values in order to prepare sheets with different transparency.

With the present set up a sub millimetre spatial resolution was possible (one pixel corresponds to approximately 0.6 sq. millimetre area of the sheet). For calculation purpose, an area of interest of 50 X 50 pixels of uniform illumination was selected as shown in **Figure 2**.

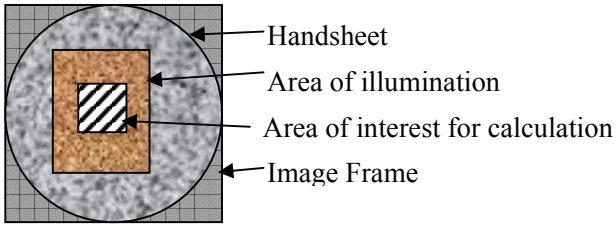

Figure 2: *Selection of an area of interest (AOI) from the image frame*

4 RESULTS AND DISCUSSION

In **Figure 3**, the temporal temperature response of one single pixel is shown along with laser pulses.

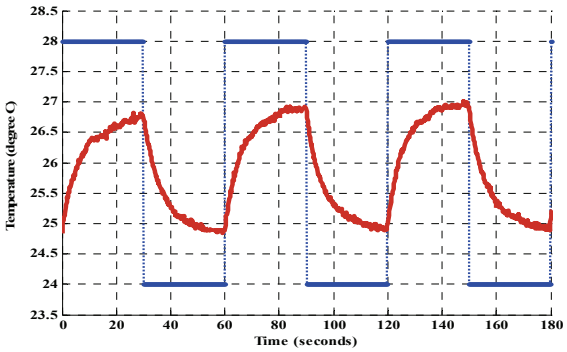

Figure 3: *Temperature response of one pixel with input laser step pulse*

This time series data for each image pixel was used for calculation in the Fourier space for the estimation of amplitude damping and phase shift at each input laser frequency. Prior to the acquisition of images, the system was allowed to reach an equilibrium state by switching the laser on and off for a few cycles. In **Figure 4** and **Figure 5**, the spectral amplitude attenuation and the phase shift is plotted against the input laser frequencies as double logarithmic plots for one example pixel. The measurements at same frequency in those figures correspond to the higher overtones of the measurement frequencies. It is possible to calculate the time constant from both of them. Since the phase shift is independent of input laser intensity fluctuation, it is more reliable (and hence recommended by almost all authors) for accurate calculation of time constant parameters. The time constant was calculated from these measurements to be ≈ 17±3 seconds.

With this value of the time constant, we are all set to calculate the heat capacity per unit area of paper from Equation (18). All other parameters are known constants or can be measured easily, (ρ_{air} = 1.2 Kgm^{-3} and c_p = 1007 JKg^{-1}K^{-1}). The emissivity of paper at the measurement wavelength was not very well known. Hence a range of values (0.7-0.9) from literature is used for the calculation and the error introduced due to this is estimated. With this, the calculated heat capacity is then (1.4 - 1.72) x 10^3 JKg^{-1} K^{-1}. This value of heat capacity is well within the literature estimated value (1.1 – 2.3 KJ Kg^{-1}K^{-1}) of heat capacity of different composition and types of paper. To ensure these values, the conventional Differential Scanning Calorimetric (DSC) measurements were carried out for the same samples. The corresponding value was (1.42 - 1.6) x 10^3 JKg^{-1} K^{-1} which ends in a maximum measurement error of up to 20 % for different paper samples.

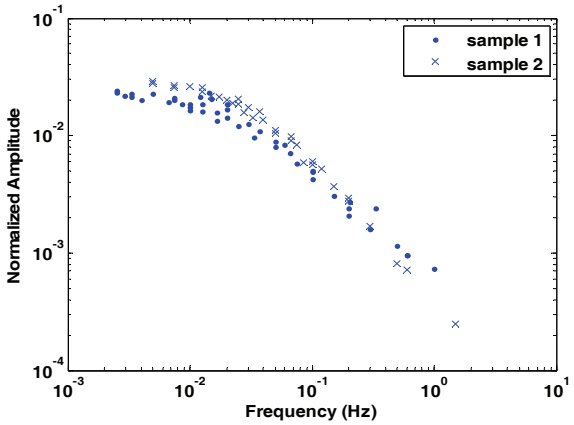

Figure 4: *Measured spectral amplitude attenuation as a function of frequency*

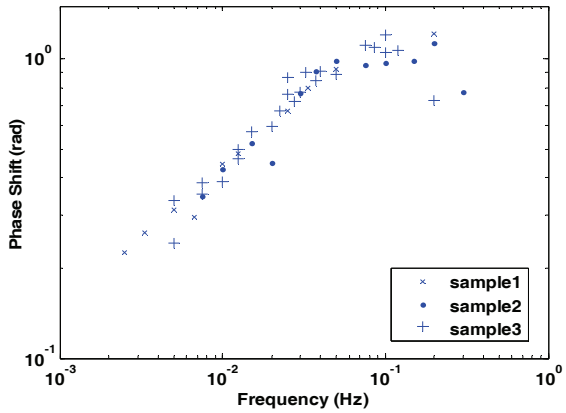

Figure 5: *Measured phase shift as a function of frequency*

In the **Figure 6** and **Figure 7**, the parameter image of amplitude damping and the phase shifts are shown for two different frequencies along with their horizontal and vertical line profile. At the low frequency of the applied heat flux, the amplitude of the temperature response is almost constant and equal to the response at a constant flux. With increasing frequency, the amplitude decreases gradually. The phase shift increases linearly with increasing frequency and then levels off at higher frequencies.

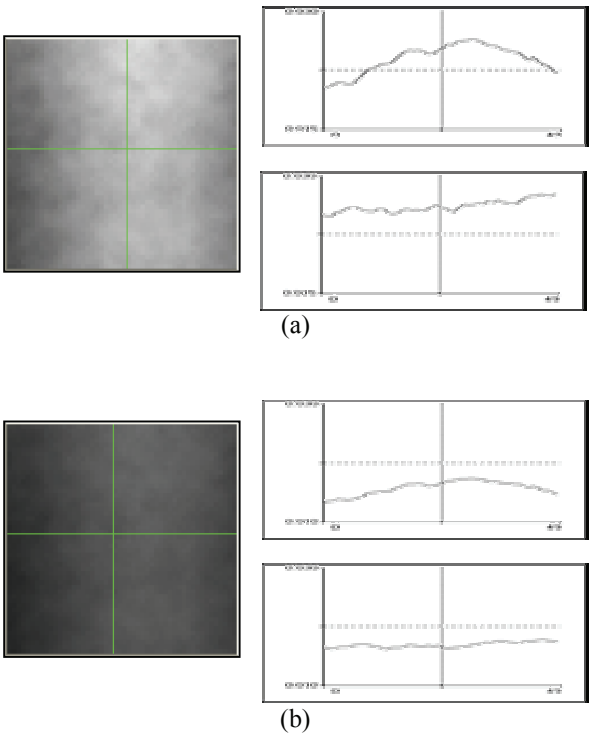

Figure 6: *Intensity image of amplitude damping with horizontal and vertical line profile at different frequency, (a) at 0.0025 Hz (b) at 0.0125 Hz*

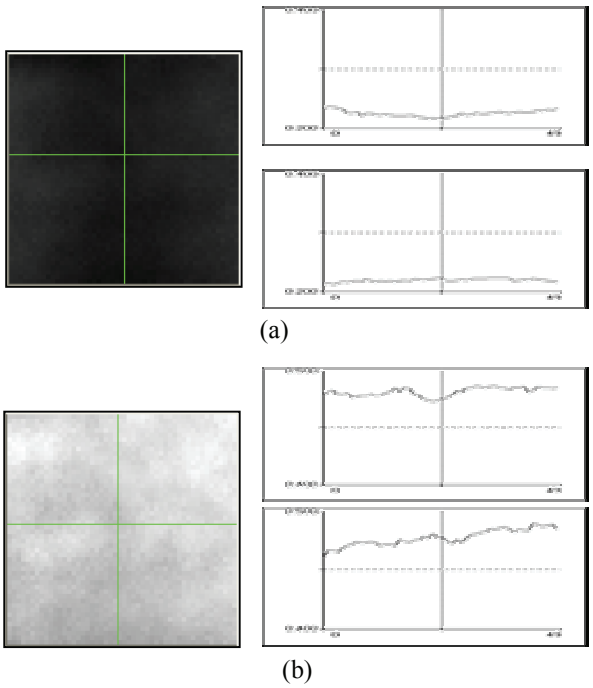

Figure 7: *Intensity image of phase shift with horizontal and vertical line profile at different frequency, (a) at 0.0025 Hz and (b) at 0.0125 Hz*

From these spatial maps of the phase shifts, a spatial distribution of heat capacity could be easily calculated and visualized. **Figure 8** and **Figure 9** are such plots for two different paper samples. The two axes in the figures correspond to the spatial coordinates of the pixels. It is also possible to calculate local heat transfer coefficient from the phase delay information [16-17].

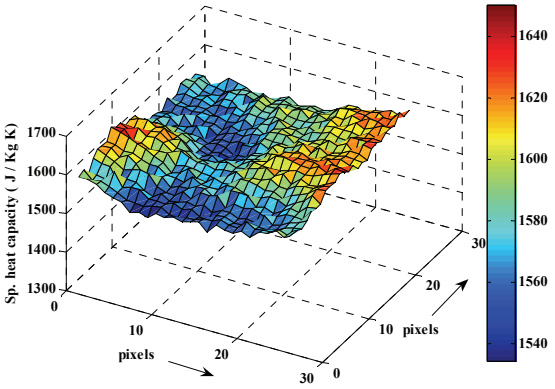

Figure 8: *Spatial distribution of heat capacity*

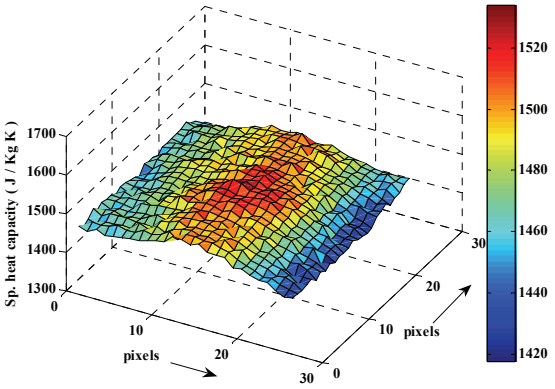

Figure 9: *Spatial distribution of heat capacity*

It is clearly visible from **Figure 8** and **Figure 9** that there exist spatial inhomogeneities in the heat capacity of paper. This distribution may depend on several factors such as structure, mass distribution and moisture content of paper. At present we are not in a position to correlate this distribution to any of the structural properties of paper, which is subject to further investigation.

5 CONCLUSIONS

With thermal image sequence analysis, two different approaches for the characterisation of thermal properties of paper sheets with high spatial and temporal resolution have been developed. The resolution is only limited by the resolution of the infrared camera and the optics. Observed

results showed good agreement with conventionally measured values. Our proposed non-invasive technique shows high potential to be used for dynamic measurements such as paper drying.

6 FUTURE WORK

Future work will be carried out to investigate the relation between the local distribution of thermal properties of paper and the structural properties e.g. mass distribution, pore size distribution and moisture content.

7 ACKNOWLEDGEMENTS

The author gratefully acknowledges the financial support from Deutsche Forschungsgemeinschaft (German Research Foundation) for this research in the framework of the Graduiertenkolleg GRK1114, "Optical Techniques for Measurement of Interfacial Transport Phenomena".

REFERENCES

1. CARLSSON, J., MALMQVIST, L., NILSSON, C.M., PERSSON, W. - *TAPPI International Paper Physics Conference,* p429(1999).
2. PUGH, Jon.F. – *Tappi J* **63**(10):131(1980).
3. SAIN, M.M., MARCHILDON, L., DANEAULT, C., PEDNAULT, C., ROBARD, S. - *Appita* **48**(5):351(1995).
4. TAYLER, David L., *Tappi J* **55**(4):563(1972).
5. SCHENTZINGER, T. - *Das Papier* May;p237(1971).
6. TAPPI ENGINEERING CONFERENCE PANEL - *Tappi J* **83**(7):48(2000).
7. KIISKINEN, H.T., KUKKONEN, H.K., PAKARINEN, P.I., LAINE, A.J. - *Tappi J* **80**(4):159 (1997).
8. ATKINS, J.W., RODENCAL, T.E., VICKERY, D.E. – *Tappi J* **65**(2):49(1982).
9. MERCER, C.- *Pulp & Paper Canada* **85**(9):13(1984).
10. CHARLES, J.A., *Tappi Engineering/Process and Product Quality Conference & Trade Fair*(1),19-17, (1999).
11. YAMAUCHI, T. and MURAKAMI, K., Japan *Tappi J* **46**(4):70 (1992).
12. FORESTER, W.K., Lobbs, T.J., US Patent no.: 5,823,677, (1998).
13. HOJJATIE, B., ABEDI, J. and COFFIN, D.W.- *Tappi J* **84**(5):1(2001).
14. JÄHNE, B., LIBNER, P., FISCHER, R., BILLEN, T., PLATE, E. J., *Tellus* **41B**:177-195, (1989).
15. GARBE, C.S., SCHURR, U. and B. JÄHNE, B., MALDAGUE, X. P. and Rozlosnik, A. E.(eds.) ThermoSense. SPIE 4710: 407, (2002).
16. WANDELT, M. and ROETZEL, W., Proceedings of Eurotherm Seminar n^{o} 50, Stuttgart, Germany, (1996).
17. TURNBULL, W.O., OOSTHUIZEN, P.H., Heat Transfer 1998, Proceedings of 11th IHTC, Vol 4, Kyongju, Korea, (1998).

SYMBOLS USED

Symbols	Description	Unit
T	temperature of paper	^{o}C
t	time	s
j	heat flux	Wm^{-2}
Q	heat energy	W
A	area	m^{2}
C	heat Capacity	JK^{-1}
α	absorptivity	cm^{-1}
σ	Stefan-Boltzmann constant	$JK^{-4}m^{-2}s^{-1}$
D	diffusion coefficient	$cm^{2}s^{-1}$
P	density	Kgm^{-3}
c_p	specific heat capacity	$KJKg^{-1}K^{-1}$
k	transfer velocity	ms^{-1}
λ	latent heat of evaporation	$KJKg^{-1}$
τ	time constant	s
ω	angular velocity	$rad\ s^{-1}$

Subscripts	Description
paper	handsheet
air	air
ir	infrared
sol	solar radiation
sen	sensible heat
lat	latent heat
net	net heat
diff	diffusion
wv	water vapour
surr	surrounding